Photoluminescence Mapping of "As-Grown" Single-Walled Carbon Nanotubes: A Comparison with Micelle-Encapsulated Nanotube Solutions

ARTICLE *in* NANO LETTERS · JANUARY 2006

Impact Factor: 13.59 · DOI: 10.1021/nl051888y · Source: PubMed

NANO LETTERS

2005
Vol. 5, No. 12
2618−2623

Photoluminescence Mapping of "As-Grown" Single-Walled Carbon Nanotubes: A Comparison with Micelle-Encapsulated Nanotube Solutions

Toshiya Okazaki,*,†,‡ Takeshi Saito,† Koji Matsuura,†,§ Satoshi Ohshima,† Motoo Yumura,† and Sumio Iijima†

Research Center for Advanced Carbon Materials, National Institute of Advanced Industrial Science and Technology (AIST), Tsukuba 305-8565, Japan, CREST, Japan Science Technology Corporation, c/o Research Center for Advanced Carbon Materials, AIST, Tsukuba 305-8565, and Japan Fine Ceramics Center, c/o Research Center for Advanced Carbon Materials, AIST, Tsukuba 305-8565

Received September 22, 2005; Revised Manuscript Received October 31, 2005

ABSTRACT

Band gap photoluminescence (PL) is observed from "as-grown" single-walled carbon nanotubes (SWNTs) in solid form. The relative PL intensities for six specific semiconducting SWNTs are compared directly to those of the micelle-encapsulated SWNTs' solutions to investigate the influence of the micelle dispersion process on PL measurements. The results indicate that sodium dodecyl sulfate (SDS) and sodium cholate (SC) selectively solubilize smaller-diameter nanotubes, whereas sodium dodecylbenzene sulfonate (SDBS) solution does not exhibit significant diameter selectivity within the diameter range studied here (d_t = 0.829–0.966 nm).

The recent discovery of band gap photoluminescence (PL) of single-walled carbon nanotubes (SWNTs) has paved a new way of investigating their unique electronic properties induced by low-dimensionality.[1,2] Especially, two-dimensional (2D) mapping of emission and excitation spectra provides rich information about electronic properties associated with optical interband transitions between van Hove singularities in both sides of the valence and conduction bands for individual (*n*, *m*) nanotubes. For practical applications, the detailed composition of the bulk samples can be deduced from PL mapping. Accurate quantitative analysis has not been achieved yet, however, because the relative PL quantum yield of specific (*n*, *m*) nanotubes is needed to estimate the composition from observed PL intensities. Furthermore, to obtain the PL spectrum, it is necessary to detach SWNTs from bundles by agitating them in micellar solution because aggregation of the tubes quenches the PL signals.[1] After the treatments, the concentration distribution of SWNTs in the micellar dispersion possibly changes from that in the as-grown material. However, an understanding of the dispersion effects on the composition change is still lacking.

Here we report the optical characterization of as-grown SWNTs in solid form by using a conventional PL measurement system. The band gap PL signals are observed successfully from as-grown SWNTs whose intensity should reflect the neat concentration of each of the (*n*, *m*) tubes in the bulk sample. The obtained results are compared directly to those of several micellar solutions of SWNTs in order to reveal the difference in SWNTs composition before and after the dispersion processes.

We investigated the dispersion characters of three surfactants: sodium dodecyl sulfate (SDS), sodium cholate (SC), and sodium dodecylbenzene sulfonate (SDBS). The SWNTs used here were synthesized by the direct-injection pyrolytic-synthesis (DIPS) method.[3] Micellar solutions of SWNTs were prepared by a procedure similar to that of Bachilo et al.[2] Briefly, as-grown SWNTs (∼1 mg) were dispersed for 10 min in ∼20 mL of D_2O containing 1 wt % of the surfactants using a 200 W homogenizer (SONICS VCX500) equipped with titanium alloy tip (TI-6AL-4V). Each solution was then centrifuged at 127 600 g for 2.5 h (HITACHI CP 100MX),

* Corresponding author. E-mail: toshi.okazaki@aist.go.jp. Tel: +81-29-861-4173. Fax: +81-29-861-4851.
† AIST.
‡ CREST.
§ JFCC.

10.1021/nl051888y CCC: $30.25
Published on Web 11/19/2005

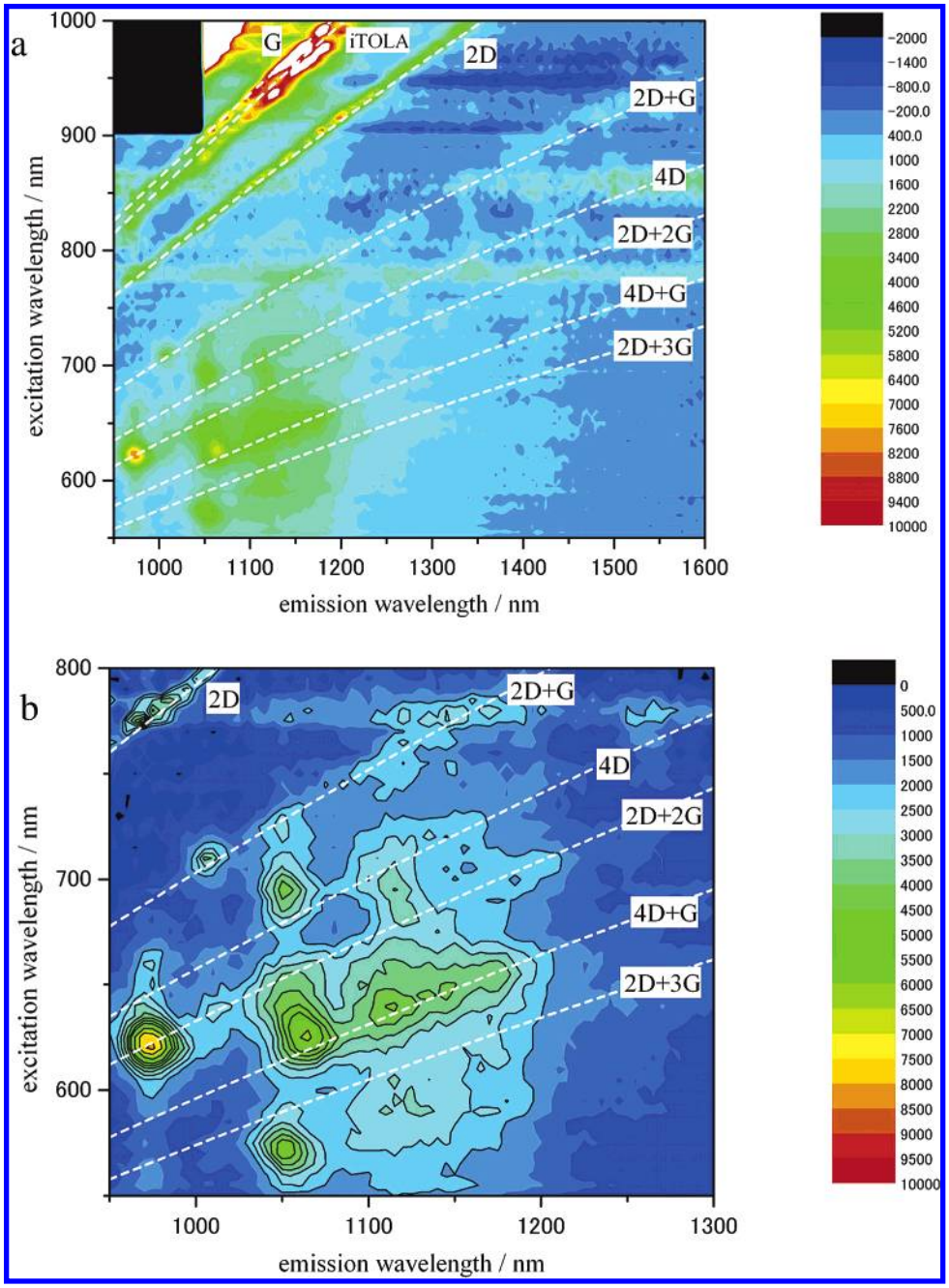

Figure 1. (a) Two-dimensional contour plots of the NIR photoluminescence mapping of as-grown DIPS-SWNTs. (b) Expanded view of the PL signal region. Dashed white lines denote the Raman modes extrapolated from previous experimental data of the graphite-related materials in the visible wavelength region.

and the supernatant of the upper ~2/3 volume was used. The natural pH level of the dispersions was at pH ≈ 8 for all three dispersions (SDS, SC, and SDBS). It is known that the PL emission from larger-diameter tubes is quenched, especially in acidic conditions.[4−6] We therefore checked that the PL intensity of the larger-diameter SWNTs did not enhance when the pH level of the dispersions increased by adding 1 N NaOH. Indeed, the 2D PL maps at pH ≈ 12 were almost identical to those of the natural pH dispersions (pH ≈ 8) within our experimental error. The optical measurements were carried out with a HORIBA SPEX Fluorolog 3-2 TRIAX spectrofluorometer equipped with a near-infrared photomultiplier module (HAMAMATSU H9170-75). The slit widths and scan steps were 7−10 nm and 3−5 nm, respectively, for both excitation and emission. The emission was collected in a backscattering geometry. The raw data were corrected for wavelength-dependent instrumental factors and excitation lamp intensities.

The 2D PL contour plot of as-grown DIPS-SWNTs as a function of emission (λ_{11}) and excitation (λ_{22}) wavelengths is shown in Figure 1a. The PL maxima (spots) on the map were seen clearly in the range of 550−720 nm excitations. An expanded view of the PL region is shown in Figure 1b. To see the individual PL peaks clearly, we draw some contour lines. Dashed white lines denote the Raman modes extrapolated from previous experimental data of the graphite-

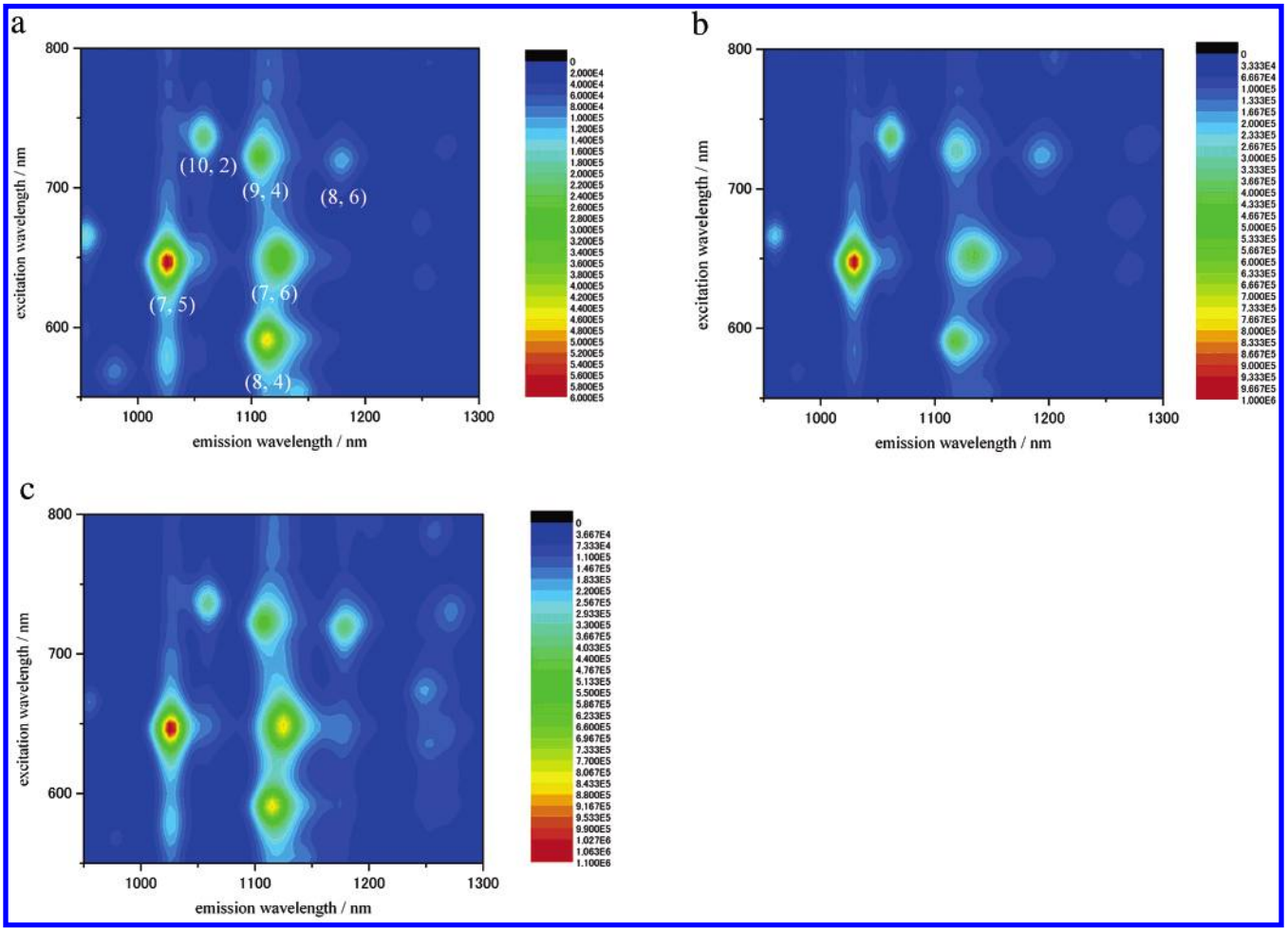

Figure 2. Two-dimensional contour plots of the NIR photoluminescence mappings of (a) DIPS-SWNTs/SDS/D_2O (pH = 8.0), (b) DIPS-SWNTs/SC/D_2O (pH = 7.9), and (c) DIPS-SWNTs/SDBS/D_2O (pH = 7.8), respectively.

Table 1. Spectral Data from the PL Map of As-Grown DIPS-SWNTs (Figure 1b)[a]

(n, m)	(7, 5)	(7, 6)	(8, 4)	(8, 6)	(9, 4)	(10, 2)
d_t/nm[b]	0.829	0.895	0.840	0.966	0.916	0.884
θ/deg[b]	24.50	27.46	19.11	25.28	17.48	8.95
E_{11}/eV	1.273	1.165	1.178	1.108	1.177	1.231
λ_{11}/nm	974	1065	1053	1119	1053	1008
ΔE_{11}/meV	62	58	62	51	51	54
E_{22}/eV	1.992	1.981	2.166	1.784	1.785	1.749
λ_{22}/nm	622	626	573	695	695	709
ΔE_{22}/meV	71	67	61	57	69	66
E_{22}/E_{11}	1.56	1.70	1.84	1.61	1.52	1.42
E_{22}/E_{11} (SDS)[a]	1.59	1.73	1.90	1.64	1.53	1.44
I_{PL}^{AG}	1	0.68	0.59	0.29	0.53	0.44

[a] The spectral parameters were obtained by the curve fitting with a Lorentzian function. [b] From ref 12.

related materials in the visible wavelength region.[7−9] These lines overlap very well with some obtained signals, indicating that the resonance Raman signals were observed coincidentally.[10,11]

The corresponding PL map of DIPS-SWNTs/SDS/D_2O is shown in Figure 2a, in which six PL spots were prominently observed. The peak positions of the PL signals were almost identical to the previous results of HiPco-SWNTs/SDS/D_2O.[12] These peaks can therefore be assigned to the emission from the first interbands (E_{11}) of (7, 5), (7, 6), (8, 4), (8, 6), (9, 4), and (10,2) tubes, respectively, following the photoexcitation to the second interband (E_{22}). Obviously, the PL peak distribution of as-grown DIPS-SWNTs (Figure 1b) is similar to that of DIPS-SWNTs/SDS/D_2O (Figure 2a). This similarity strongly suggests that the origins of the PL peaks in Figure 1b are the same as those of the corresponding peaks in Figure 2a.

Comparing to the SDS-encapsulated SWNTs, the emission and excitation peaks for as-grown DIPS-SWNTs are uniformly blue-shifted. If bundled SWNTs could provide PL

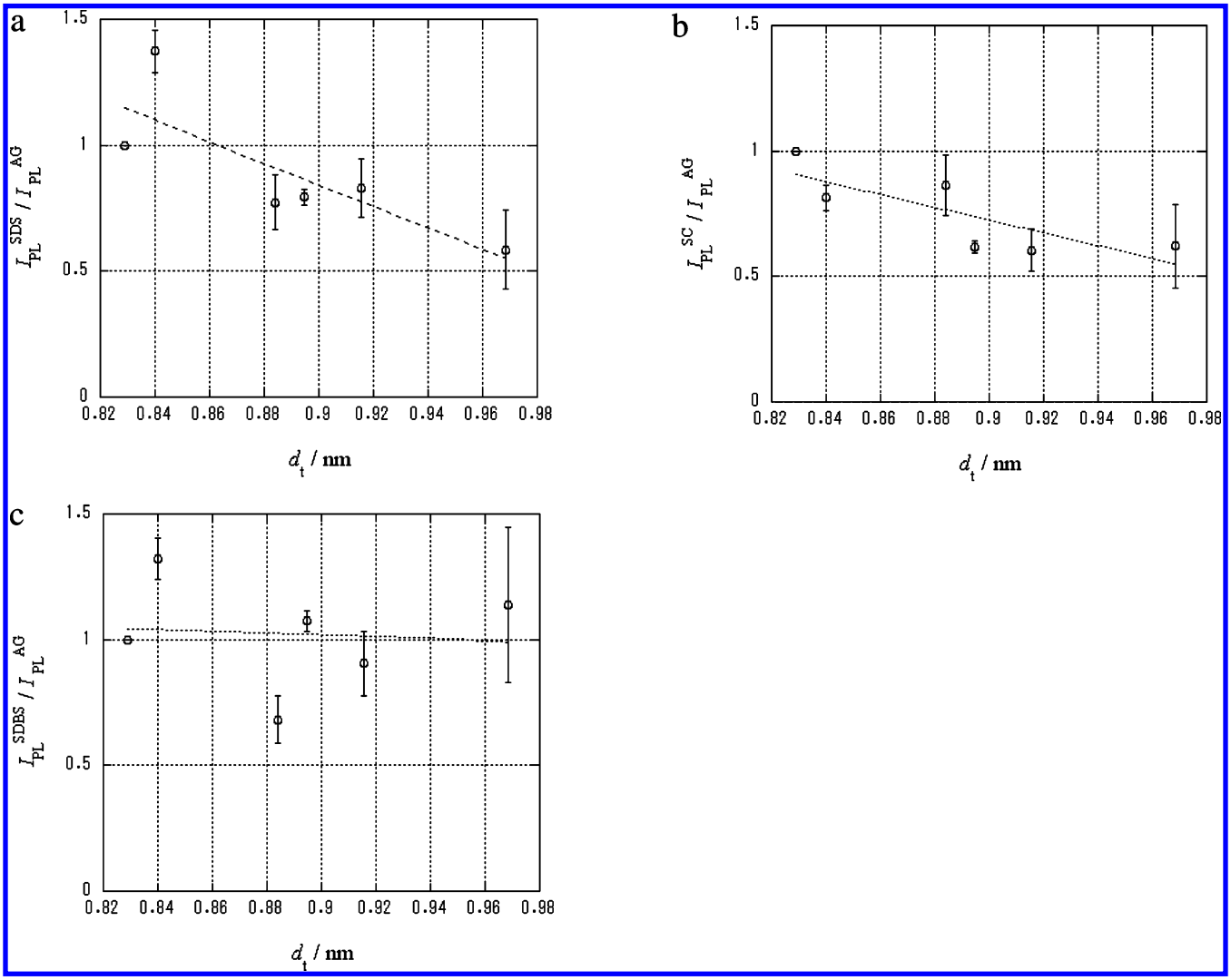

Figure 3. PL intensity ratio between (a) DIPS-SWNTs/SDS/D_2O and as-grown DIPS-SWNTs, (b) DIPS-SWNTs/SC/D_2O and as-grown DIPS-SWNTs, and (c) DIPS-SWNTs/SDBS/D_2O and as-grown DIPS-SWNTs as a function of tube diameter (d_t). The dotted lines denote the square least fitting results.

signals, then the peak positions might be red-shifted.[13,14] Thus, it is likely that the observed PL signals in Figure 1b originated from individual SWNTs in the bulk sample. The spectral parameters for each PL peak of as-grown DIPS-SWNTs obtained by the curve fitting with a Lorentzian function are listed in Table 1. The average values of the relative shifts in emission ($\Delta E_{11}/E_{11}$) and excitation ($\Delta E_{22}/E_{22}$) between as-grown DIPS-SWNTs and the SDS solution were 4.8 and 3.5%, respectively. These values are similar to, but slightly larger than, those obtained for air-suspended SWNTs between pillars (3.0 and 1.0% for $\Delta E_{11}/E_{11}$ and $\Delta E_{22}/E_{22}$, respectively).[15] It is well known that the transition energy is very sensitive to the local environment. The obtained small deviations in $\Delta E_{11}/E_{11}$ and $\Delta E_{22}/E_{22}$ could arise from the structural differences between the present and the previous samples. Furthermore, it is worth noticing that the E_{22}/E_{11} ratios for the as-grown DIPS nanotubes are slightly lower than those of the SDS-encapsulated SWNTs. A similar tendency was observed for the SWNTs suspended between pillars.[15] These results suggest that substantial amounts of suspended nanotubes existed in as-grown DIPS-SWNTs. In fact, once we made a "Bucky paper" from as-grown DIPS-SWNTs by filtration of the ethanol dispersion, the PL signals were severely depressed, probably because of the formation of the thick bundles.

Normally, as-grown SWNTs contain few isolated tubes. Most SWNTs constitute bundle structures because of van der Waals forces. The reason that the present DIPS sample has so many isolated SWNTs can be explained as follows. In the DIPS method, SWNTs were produced in the gas phase, flowed out of a hot zone of the furnace with the carrier gas stream within 2 s, and accumulated in the collection part that is located at the bottom of the reactor tube.[3] The extremely short stay (less than ~2 s) inside the hot zone prevents bundles from forming during the reaction. Consequently, considerable amounts of individual SWNTs were accidentally suspended between the other SWNTs or amorphous carbons (impurities).

Although the PL quantum yield is not applied for correction, the relative PL intensity of as-grown DIPS-SWNTs

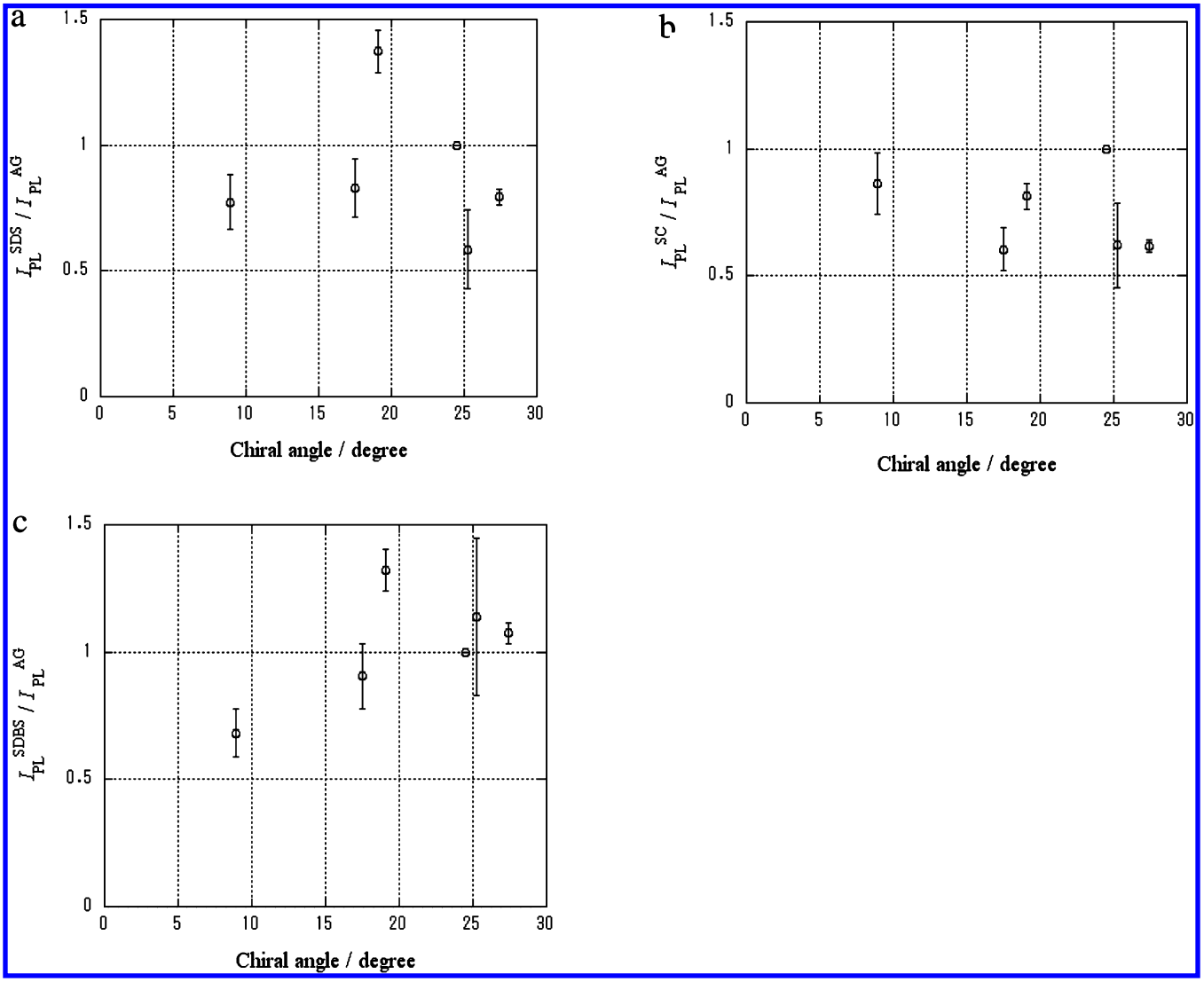

Figure 4. PL intensity ratio between (a) DIPS-SWNTs/SDS/D_2O and as-grown DIPS-SWNTs, (b) DIPS-SWNTs/SC/D_2O and as-grown DIPS-SWNTs, and (c) DIPS-SWNTs/SDBS/D_2O and as-grown DIPS-SWNTs as functions of a chiral angle of SWNTs.

(I_{PL}^{AG}) should reflect the concentration distribution of SWNTs in the bulk sample. The obtained I_{PL}^{AG} by curve fitting are listed in Table 1, where each of the PL intensities was normalized by that of the (7, 5) tube. To clarify the influence of the dispersion process on the composition of SWNTs, we compared the relative PL intensities of as-grown DIPS-SWNTs with those of micelle-encapsulated DIPS-SWNTs. Figure 3a shows that the ratio between the relative intensities of SDS-encapsulated SWNTs and as-grown SWNTs (I_{PL}^{SDS}/I_{PL}^{AG}) as a function of the diameter of SWNTs (d_t). If the compositions are similar between the as-grown and the SDS-encapsulated SWNTs, then the values should become $I_{PL}^{SDS}/I_{PL}^{AG} = 1$. Even though a close similarity of the PL peak pattern was observed between as-grown and SDS dispersion of DIPS-SWNTs (Figures 1b and 2a), it is apparent that I_{PL}^{SDS}/I_{PL}^{AG} decreases gradually with increasing diameter of the tube, indicating that SDS preferentially dissolves the smaller-diameter tubes rather than the larger-diameter SWNTs. The same trend was also observed in the SC micellar solution case (Figures 2b and 3b). The relative PL intensity of SWNTs with larger diameters in the SC micellar solution was depressed as compared to as-grown DIPS-SWNTs.

Alternatively, such diameter dependence was inconspicuous in the same plot of the SDBS solution of DIPS-SWNTs (Figures 2c and 3c). The values of $I_{PL}^{SDBS}/I_{PL}^{AG}$ seem to be less sensitive to the diameter of SWNTs. The slope of the square least fitting line is almost flat. The observed behavior is consistent with the previous result, in which large-diameter PLV nanotubes ($d_t \approx 1.2-1.4$ nm) were dispersed more efficiently in SDBS/D_2O in comparison to SDS/D_2O.[16]

Generally, solubility of molecules decreases as the molecular size increases. One of the possible reasons for the solubulizing capability of SDBS for larger-diameter nanotubes may be due to the $\pi-\pi$ interactions between benzene ring moieties.[17] It is believed that the SDBS molecules adsorbed on the surface with a vertical orientation with the anionic headgroups directed outward to the aqueous phase, which means that the benzene rings locate on the water side.[18] In this situation, it is likely that overlapping of the benzene rings increases in thicker nanotubes with flatter graphitic

surfaces, which may help to form a stable complex. For example, an ordered mesoporous structure can be synthesized with the aid of hydrophobic $\pi-\pi$ interactions between benzene rings.[19] Such an effect cannot be expected for SDS and SC because of the lack of phenyl rings.

Nanotube structure is determined uniquely by a pair of diameter and chiral angle (θ). Interestingly, no PL signal of zigzag tubes ($\theta = 0°$) was observed in the present PL measurements. Similar results were also obtained in previous PL studies of SWNT aqueous solutions[2,12] except for a few cases.[20] Under these circumstances, the chiral angle dependence on the dispersion processes is particularly intriguing to study. We therefore plot the ratios of the relative PL intensities of three micellar solutions to those of as-grown SWNTs (I_{PL}^{SDS}/I_{PL}^{AG}, $I_{PL}^{SDBS}/I_{PL}^{AG}$, and I_{PL}^{SC}/I_{PL}^{AG}) as a function of the chiral angle of SWNTs (Figure 4). It seems that these values do not depend on the chiral angle of the SWNTs for these micellar solutions. The dispersion process is insensitive to the chiral angle of the SWNTs, at least within the sample ($\theta = 9-27°$).

We should note here that the energy transfer form smaller-diameter nanotubes to larger-diameter tubes in nanotube bundles was neglected in the present analysis, which may enhance the PL signals of SWNTs with larger diameters. Although the details of the energy transfer process have not yet been eliminated, the line shape of the spectrum may be affected by the process. The PL signals observed here can be fitted well by a Lorentzian function with average line widths of 32, 26, 28, and 26 meV for AG-SWNTs, SDS, SC, and SDBS solutions, respectively. These values are consistent with the widths that can be interpreted as inhomogeneous broadening within a single tube, whereas bundled nanotubes show more broad and diffuse spectra.[21] Hence, it is likely that the energy transfer process in nanotube bundles does not affect the present observations significantly.

Our present findings reveal that the dispersion process is crucial to determining the content of each of the SWNTs in the bulk sample by the PL measurement. Direct observation of the PL signal from as-grown SWNTs without any treatment allowed us to examine the dispersion effect quantitatively. To facilitate quantitative analysis of SWNTs, it is necessary for one to find an appropriate surfactant that does not affect the nanotube composition during the dispersion processes. Although the present measurements were carried out within limited diameters ($d_t = 0.829-0.966$ nm), SDBS was found to be one of the plausible candidates. However, it was surprising that SDS and SC can discriminate a diameter difference of SWNTs with subnanometer sensitivity ($\sim$0.1 nm). Such diameter-selective solubility of SDS and SC may be utilized for separation and isolation of SWNTs with a specific chirality.

Acknowledgment. We thank K. Suenaga, T. Yamada, H. Yokoi, Y. Ikeda, and S. Kazaoui for their helpful discussions and experimental supports.

References

(1) O'Connell, M. J.; Bachilo, S. M.; Huffman, C. B.; Moore, V. C.; Strano, M. S.; Haroz, E. H.; Rialon, K. L.; Boul, P. J.; Noon, W. H.; Kittrell, C.; Ma, J.; Hauge, R. H.; Weisman, R. B.; Smalley, R. E. *Science* **2002**, *297*, 593.
(2) Bachilo, S. M.; Strano, M. S.; Kittrell, C.; Hauge, R. H.; Smalley, R. E.; Weisman, R. B. *Science* **2002**, *298*, 2361.
(3) Saito, T.; Ohshima, S.; Xu, W.-C.; Ago, H.; Yumura, M.; Iijima, S. *J. Phys. Chem. B* **2005**, *109*, 10647.
(4) Strano, M. S.; Huffman, C. B.; Moore, V. C.; O'Connel, M. J.; Haroz, E. H.; Hubbard, J.; Miller, M.; Rialon, K.; Kittrell, C.; Ramesh, S.; Hauge, R. H.; Smalley, R. E. *J. Phys. Chem. B* **2003**, *107*, 6979.
(5) Weisman, R. B.; Bachilo, S. M.; Tsyboulski, D. *Appl. Phys. A* **2004**, *78*, 1111.
(6) Dukovic, G.; White, B. E.; Zhou, Z.; Wang, F.; Jockusch, S.; Steigerwald, M. L.; Heinz, T. F.; Friesner, R. A.; Turro, N. J.; Brus, L. E. *J. Am. Chem. Soc.* **2004**, *126*, 15269.
(7) Tan, P. H.; Tang, Y.; Deng, Y. M.; Li, F.; Wei, Y. L.; Cheng, H. M. *Appl. Phys. Lett.* **1999**, *75*, 1524.
(8) Tan, P.-H.; Hu, C.-Y.; Dong, J.; Shen, W.-C.; Zhang, B.-F. *Phys. Rev. B* **2001**, *64*, 214301.
(9) Saito, R.; Grüneis, A.; Samsonidze, G. G.; Brar, V. W.; Dresselhaus, G.; Dresselhaus, M. S.; Jorio, A.; Cancado, L. G.; Fantini, C.; Pimenta, M. A.; Filho, A. G. S. *New J. Phys.* **2003**, *5*, 157.
(10) Chou, S. G.; Plentz, F.; Jiang, J.; Saito, R.; Nezich, D.; Ribeiro, H. B.; Jorio, A.; Pimenta, M. A.; Samsonidze, G. G.; Santos, A. P.; Zheng, M.; Onoa, G. B.; Semke, E. D.; Dresselhaus, G.; Dresselhaus, M. S. *Phys. Rev. Lett.* **2005**, *94*, 127402.
(11) Htoon, H.; O'Connell, M. J.; Doorn, S. K.; Klimov, V. I. *Phys. Rev. Lett.* **2005**, *94*, 127403.
(12) Weisman, R. B.; Bachilo, S. M. *Nano Lett.* **2003**, *3*, 1235.
(13) Fantini, C.; Jorio, A.; Souza, M.; Strano, M. S.; Dresselhaus, M. S.; Pimenta, M. A. *Phys. Rev. Lett.* **2004**, *93*, 147406.
(14) O'Connell, M. J.; Sivaram, S.; Doorn, S. K. *Phys. Rev. B* **2004**, *69*, 235415.
(15) Lefebvre, J.; Fraser, J. M.; Homma, Y.; Finnie, P. *Appl. Phys. A* **2004**, *78*, 1107.
(16) Lebedkin, S.; Arnold, K.; Hennrich, F.; Krupke, R.; Renker, B.; Kappes, M. M. *New J. Phys.* **2003**, *5*, 140.
(17) Lin, Y.; Taylor, S.; Li, H.; Fernando, K. A. S.; Qu, L.; Wang, W.; Gu, L.; Zhou, B.; Sun, Y.-P. *J. Mater. Chem.* **2004**, *14*, 527.
(18) Matarredona, O.; Rhoads, H.; Li, Z.; Harwell, J. H.; Balzano, L.; Resasco, D. E. *J. Phys. Chem. B* **2003**, *107*, 13357.
(19) Inagaki, S.; Guan, S.; Ohsuna, T.; Terasaki, O. *Nature* **2002**, *403*, 304.
(20) Chou, S. G.; Ribeiro, H. B.; Barros, E. B.; Santos, A. P.; Nezich, D.; Samsonidze, G. G.; Fantini, C.; Pimenta, M. A.; Jorio, A.; Filho, F. P.; Dresselhaus, M. S.; Dresselhaus, G.; Saito, R.; Zheng, M.; Onoa, G. B.; Semke, E. D.; Swan, A. K.; Ünlü, M. S.; Goldberg, B. B. *Chem. Phys. Lett.* **2004**, *397*, 296.
(21) Tsyboulski, D. A.; Bachilo, S. M.; Weisman, R. B. *Nano Lett.* **2005**, *5*, 975.

NL051888Y